Egypt. J. Chem. **Vol. 64**, No. 10 pp. 5839 – 5852 (2021)

Egyptian Journal of Chemistry

http://ejchem.journals.ekb.eg/

Electrochemical Sensing of Dissolved Oxygen at Ternary Graphene Composite Modified Glassy Carbon Electrode

Kh. El-Sayed[a, c,*] Z. Abdel Hamid[b], Taher A. Salah Eldin[c,f], H. B. Hassan[d], Sayed Sabet Abd El Rehim[e]

[a] *Nanotechnology Research Center, British University in Egypt(BUE).*

[b] *Corrosion Control and Surface Protection Laboratory, CMRDI, Helwan, Cairo, Egypt.*

[c] *Nanotechnology & Advanced Materials Central Lab, Agricultural Research Center, Giza, Egypt.*

[d] *Faculty of science, Cairo University, Giza, Egypt.*

[e] *Chemical Department, Faculty of science, Ain shams university, Cairo 11566, Egypt.*

[f] *Pharmaceutical Research Institute, Albany Collage of Pharmacy and Health sciences, NY, USA.*

Abstract

Novel sensor for dissolved oxygen (DO) centered on ternary composite of graphene/titanium dioxide/silver nanoparticle (G-TiO_2-Ag) enhanced glassy carbon electrodes can be investigated. This modified composite was created using a hydrothermal process and then placed on the surface of the glassy carbon (GC) electrode as an active material. The electrochemical behavior of the GC/G-TiO_2 modified electrode in 0.1 M PBS displayed two steps four electrons (4e`) mechanism for DO reduction, while, the electrochemical behavior of GC/G-$TiO_2$-Ag displayed only one obvious peak which strongly indicates a fast and efficient one step (4e`) mechanism for DO reduction. A higher reduction current is obtained for DO on GC/G-TiO_2-Ag compared with that on GC/G-TiO_2 reflects a synergistic effect between Ag and TiO_2. The amperometric measurement showed two linear regions, the first one is from 1 to 30.29 µM with sensitivity of 1.363 μAcm^{-2} μM^{-1} and detection limit of 0.011 µM (signal/noise = 3/1) and a correlation coefficient of 0.996. The second linear region shows an increase in response, with low rate than the first region, for DO concentration up to 100 µM (correlation coefficient 0.990) with sensitivity of 0.725 μAcm^{-2} μM^{-1} and detection limit of 0.214 µM.

Keywords: Electrochemical sensor; Dissolved oxygen; Graphene composites; Chemically modified electrodes.

1. Introduction:

The determination of dissolved oxygen (DO) is an important parameter for the indication of water quality for aquaculture farming and for various physiological and biochemical parameters, such as the monitoring of DO in cell culture and in vivo study, is considered to be one of the most important requirements. DO apply to non-compound oxygen and free in water or some other solution [1-5]. Different detection methods are used for this purpose such as fluorescence [6], chemiluminescence [7], and colorimetry [8]. Recently, the researchers pay attention for using the electrochemical technique in dissolved oxygen detection. The electrochemical techniques take the advantage over the solid electrodes which suffer from slow kinetic and high potential requirement. On the other hand, the electrochemical techniques have a high sensitivity, selectivity, low cost, and fast response [9-12]. The electrode surface materials play an important role in the detection process as it affects the catalytic activity and the efficiency of electron transfer process. A lot of materials are used for such purpose such as; supramolecular complex [13], Nickel salen film [2], Manganese (II) phthalocyanine /porous SiO_2/SnO_2 [14], cobalt complexes [15], palladium-carbon nanotube [16], carbon nanotube [17, 18], nano platinum compo [3, 19-22], and gold nanoparticles

*Corresponding author: e-mail: forzeinab@yahoo.com

Receive Date: 26 March 2021, Revise Date: 19 May 2021, Accept Date: 31 May 2021

DOI: 10.21608/EJCHEM.2021.69425.3525

[23]. Also, noble metals, doped with metal oxides (like MnO_2, TiO_2, WO_3, CeO_2 and Fe_2O_3), have been showed obvious enhancement in the performance of the oxygen reduction [24, 25]. TiO_2 has an enhancing effect on many oxidation and reduction reactions in electrochemical energy conversion systems. This is due to the hypo-d-electron character that makes strong interactions with hyper-d-electron character metals [26]. As a result, the inhibition of hydroxyl chemisorption and the shift of the formation of surface MOH toward positive potentials are observed, and these likely increase the interaction with molecular oxygen in the oxygen reduction reaction (ORR). Moreover, Ag and Ag-based materials are a promising catalyst for ORR due their low cost and prospective electrocatalytic activity. Ag possesses properties that other noble metals do not (e.g., Pt, Au and Pd), Ag is maintained in its metallic state during ORR, demonstrates excellent intermediates elimination and weak binding of ORR intermediates [27-30]. The ORR mechanism and electrocatalytic activity of the Ag catalysts depend on the Ag particle size, morphology, catalyst loading, the type of facets of Ag, the catalyst support, nano alloying and pH [28, 31, 32]. It was reported that ORR on small Ag particles supported on carbon (4.1 nm) showed a two-electron pathway, while a four-electron pathway is preferred at large particles (174 nm) [33]. Silver nanoparticles deposited onto graphene showed a 4-electron reduction of oxygen [34, 35]. Also, the ORR on nitrogen-doped graphene oxide supported silver nanoparticles (Ag/NGO) catalysts synthesized by chemical reduction method occurred via 4-electron pathway yielding water, while it showed lower than 4-electron on NGO [36]. The employment of nanomaterials becomes highly critical for many applications, including sensors and biosensors, catalysis, etc. These materials provide enormous binding sites, high porosity, and rich surface textural that plays a significant role on the adsorption and chemical reaction occur at the surface and /or interface in sensor. Moreover, the highly small size of nano-materials favors the transportation kinetics and charge transfer [37-39].

Nano-carbon materials and especially graphene has drawn plenty of interest in the electrochemical sensing due to its large surface area, good electrical conductivity, high charge carrier mobility and excellent electrocatalytic properties[40-43]. In addition, graphene composites with metal and metal oxides have showed up a promising contribution in electrochemical sensing applications by enhancing the electron transfer efficiency and electrocatalytic performance. Many such composites are reported as electrode materials such as; bismuth (III) oxide/ reduced graphene oxide (RGO) [44], Graphene Oxide/Nickel-gold nanoparticles EG/Ni-Au (NPs) [45] , molybdenum disulfide/graphene [46], Graphene Oxide-Poly glycine-Cupper nanoparticle (GO/P-Gly/Cu) [47], graphene-zinc oxide composite [48], gadolinium(III) oxide/RGO [49], cerium oxide (CeO_2)/RGO hybrids [50], gold nanoparticles @ CeO_2/RGO nanocomposites [51], and so on.

In this paper, our research protocol is focused on tailoring an efficient nano-sized catalyst for DO sensing with high sensitivity and low detection limit to substitute the highly cost Pt catalyst and minimize the overpotential of ORR. A modified glassy carbon electrode covered with a thin film of graphene/titanium dioxide/silver nanoparticles (G-TiO_2-Ag) was prepared and used as a sensor for detection of dissolved oxygen. The G-TiO_2-Ag nanocomposite was fabricated through hydrothermal method, then fixed on the glassy carbon electrode surface as an active material then applied as a dissolved oxygen electrochemical sensor.

2. Experimental

2.1. Material and reagents

Graphite powder (Alfa-Aesar, Germany), Titanium (IV) isopropoxide (TTIP) (Sigma-Aldrich), Silver nitrate ($AgNO_3$) (Alfa-Aesar, Germany), ammonia solution (33% Fluka), sodium nitrate ($NaNO_3$) (Sigma-Aldrich), Sulphuric acid (95–97%, H_2SO_4) (Sigma-Aldrich), tri-Sodium citrate ($Na_3C_6H_5O_7$), hydrogen peroxide (30% H_2O_2) and potassium permanganate ($KMnO_4$) (Sigma-Aldrich). Sodium phosphate dibasic dihydrate (Na_2HPO_4. $2H_2O$) and potassium phosphate monobasic dehydrate (KH_2PO_4. H_2O) (Sigma Aldrish) were used.

2.2. Apparatus and electrochemical measurements

X-ray diffraction (XRD) was carried out to confirm the crystal structure of the prepared nanomaterial over diffraction angle 2θ (4^o- 80^o) (X'Pert PRO- PANalytical, Netherlands) and high

intensity Cu Kα (λ = 1.5404 Å) irradiation with scan speed of 0.05 s^{-1} and step size 0.02°. Studying the shape and size of the prepared nanoparticles were examined by transmission electron microscope (TEM) (TECNAI G2 S-twin, FEI). FTIR studies were obtained using Bruker (Vertex 70) FTIR for all prepared nanomaterials using the ATR unit attached to the system. The field emission scanning electron microscope (FESEM) (Quattro S, Thermo scientific) was used for examining the surface morphology of the electrode. Energy dispersive X-ray spectroscopy (EDX) and mapping analysis were performing to confirm the elemental analysis and distribution for modified electrode surface.

The electrochemical behavior study was performed on Iviumstat, The Netherlands, with a three-electrode cell (commercially manufactured). Here the bare glassy carbon electrode (GCE) each of diameter 3 mm, EDAQ Company, G-TiO_2 and G-TiO_2-Ag modified GCE were adapted as working electrodes, respectively. Calomel electrode (Hg/Hg_2Cl_2, SCE, E^o= 260 mV) is used as a reference and Platinum (Pt) wire is used as a counter electrode. Measurements have been carried out in PBS (pH 7.0) at room temperature of 25 °C. Before electrochemical measurements, the glassy carbon electrodes were mechanically polished using emery papers of various grades, and then they were subsequently degreased with acetone, rinsed with triply distilled water of conductivity 0.06 µS/cm and dried with a soft tissue paper.

For testing the electrochemical response of the glassy carbon electrode and the modified electrodes, the solution was purged with pure nitrogen gas for 30 min. For O_2 concentration determination, an aliquot of O_2-saturated solution was added to the solution using micropipette followed by stirring. O_2- saturated solution was prepared by purging distilled water with pure O_2 for 1hr that gives O_2 content in the saturated water 2.6 $\times 10^{-4}$ $molL^{-1}$ calculated from its saturated solubility [11, 52].

2.3. Fabrication of dissolved oxygen sensor

2.3.1. Synthesis of graphene- Titanium dioxide (G-TiO_2)

Graphene–titanium dioxide (G-TiO_2) was prepared using the hydrothermal method. Briefly, 0.1 g graphene oxide was dispersed in 60 ml ultra-pure Milli-Q water for 1 hr. 0.4 ml titanium tetra-isopropoxide (TTIP) was added to graphene oxide solution under stirring then under sonication for 30 min. The pH was adjusted to 4 using ammonia solution, and then the solution is transferred to Teflon-lined stainless-steel autoclave which left in the oven at 170 °C for 24 hrs. The composite was separated and washed using the centrifuge and dried at 80 °C for 12 hr. The graphene only was prepared using the same hydrothermal method without adding (TTIP) [53].

2.3.2. Preparation of Graphene –Titanium dioxide –Silver (G-TiO_2-Ag)

In this experiment, 0.03 g graphene oxide (GO) was dispersed in 50 mL deionized water (DIW), then the solution (soln. 1) was sonicated for 30 min. 0.017 g silver nitrate ($AgNO_3$) was added to the (soln. 1) under continuous stirring to form (soln. 2). The solution (soln. 2) was kept under stirring for 15 min. and 0.1 mL TIPP was added to (soln. 2) under vigorous stirring and sonication for 30 min/each to form (soln. 3). (Soln. 3) was then transferred to stainless steel autoclave and placed in oven at 180 °C for 24 hrs. The precipitate was centrifuged and dried at 80 °C for 8 hrs [54, 55].

2.3.3. Modification of GCE

The GCE surface was polished to be shining like a mirror with 0.1 and 0.05 µm alumina slurry sequentially, then sonicated to remove the adsorbed species by ethanol-water solution (1:1, v/v ratio) then with deionized water [56, 57]. Using the drop-coating method, 10 mg of each composite (G-TiO_2 and G-TiO_2-Ag) was dispersed separately in 1 ml of 5% Nafion/ethanol and sonicated for 1 h. Then 5 µL of the suspension was dropped on GCE surface and dried at room temperature in air [10, 58].

3. Results and discussion

3.1. Characterization of (G-TiO_2 and G-TiO_2-Ag)

The crystal structure of the prepared nanomaterials was confirmed using XRD as shown in Fig. 1a. The corresponding diffraction peak of graphene (G) at 24.5° with (002) plane does not appear, it could be shielded by the strong diffraction peak of TiO_2 (anatase) which appears at 25.3° with (101) plane [53, 59, 60]. The other diffraction peaks appear in the

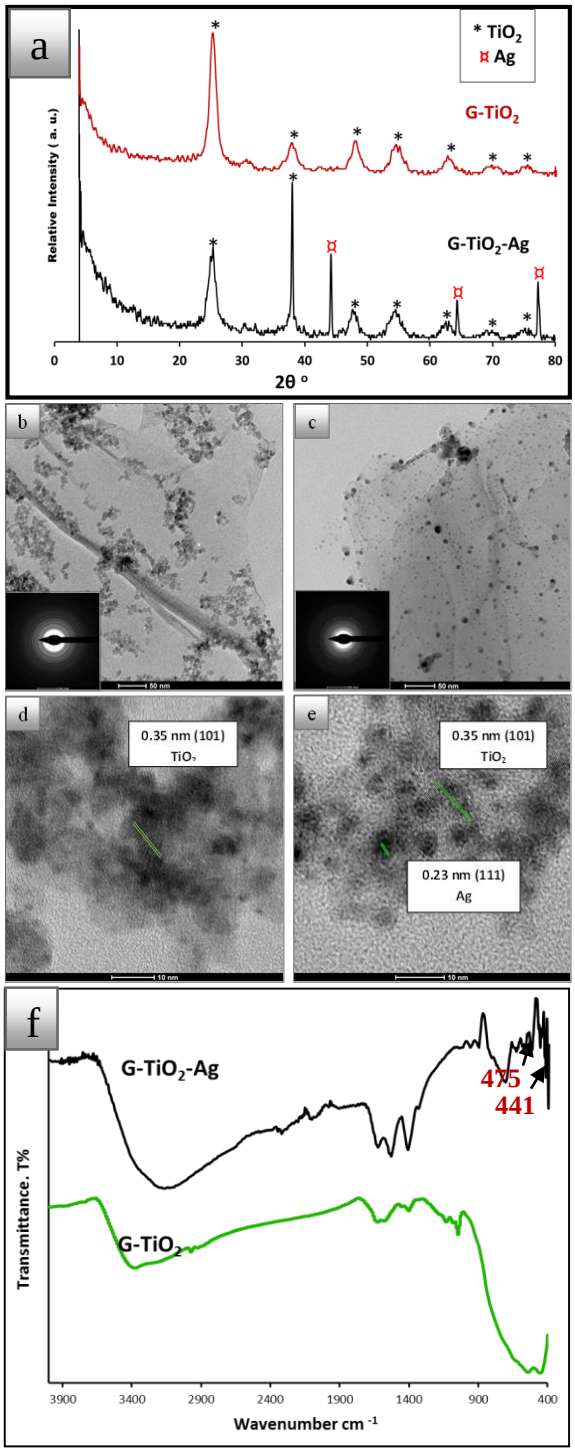

Figure 1. a) XRD patterns for G-TiO_2 and G-TiO_2-Ag nanocomposites. (b-e) HR-TEM images for b) G-TiO_2, c) G-TiO_2-Ag. d) The lattice spacing for TiO_2 in G-TiO_2 nanocomposite, e) The lattice spacing for TiO_2 and Ag in G-TiO_2-Ag nanocomposites, and f) FTIR spectra for G-TiO_2 and G-TiO_2-Ag.

patterns of G-TiO_2 and G-TiO_2-Ag refer to anatase TiO_2 according to (ICDD 01-75-2547) pattern at 2θ values of 25.3°, 37.8°, 48.0°, 54.0°, 55.1°, 62.7°, 68.8°, 70.3° and 75.1° that could be attributed to (101), (004), (200), (105), (211), (204), (116), (220) and (215) crystallographic planes of anatase phase, respectively [53]. In G-TiO_2-Ag, the diffraction peaks for anatase TiO_2 phase appear at the same 2θ values according to (ICDD 01-75-2547) pattern. Another diffraction peaks were observed for silver nanoparticles at 2θ of 38.18°, 44.25°, 64.72°, and 77.40° which were indexed to the (111), (200), (220), and (311) crystal planes of Ag nanoparticles, according to (ICDD 01-087-0719) [61]. The dramatic increase in the diffraction peak of TiO_2 at 37.8° for (004) plane, in G-TiO_2-Ag pattern compared with one in G-TiO_2 pattern, could be referred to the presence of diffraction peak of (111) plane of Ag at 38.18° near to the one of the TiO_2 which causes intensity duplication.

The particle size and shape of the prepared nanomaterials were investigated using HRTEM. In Fig. 1b, it shows the TiO_2 nanoparticles with size range from 5 to 10 nm distributed over the graphene sheet. The inset image shows the selected area electron diffraction (SAED) pattern confirming the presence of anatase TiO_2 crystal structure with planes (101), (004), (200), (105), and (211) which is matched with ICDD 01-75-2547 standard pattern for XRD. In Fig. 1c, TiO_2 and Ag nanoparticles are distributed over the graphene sheet and the size Ag nanoparticles is about 5 nm of high contrast than that of TiO_2 nanoparticles (NPs). The inset SAED pattern shows the diffraction planes for TiO_2 and Ag. The diffraction pattern for Ag particles confirms the (111), (200), (220), and (311) crystal planes that appeared in XRD diffraction peaks and matches ICDD 01-087-0719 standard pattern for Ag nanoparticles. Fig. 1d shows the lattice of TiO_2 the graphene sheet. The presence of TiO_2 and Ag nanoparticles is clearly confirmed in Fig. 1e which shows TiO_2 and Ag NPs lattice spacing structure of 0.35 nm and 0.25 nm refers to (101) and (111) plane for anatase TiO_2 and Ag nanoparticles, respectively.

FTIR spectra of G-TiO_2 and G-TiO_2-Ag are presented in Fig. 1f. It shows transmission bands at the range from 450 to 900 cm^{-1} and the band showed at 1616 cm^{-1}, is assigned to Ti-O-Ti and Ti-O-C stretching vibration modes [53, 62-65]. The bands in the range from 3200 to 3400 cm^{-1} are assigned to the stretching of the hydroxyl group of the adsorbed water on the surface of the materials[64-66]. The band appeared at 441 cm^{-1} and at ~ 475 cm^{-1} were considered as a characteristic peaks for Ag and Ag-O

stretching modes[66, 67]. The peak at around 1475 cm^{-1} is for the carboxyl group [63, 64].

The field emission scanning electron microscope is used to give the surface morphology of GC/G-TiO_2 and GC/G-TiO_2-Ag modified electrode Fig. 2). As shown in Fig. 2(a and b), illustrates a complete coverage of the glassy carbon electrode with both materials. Figure 3 (a and b) shows a magnified image for the both surfaces and in Fig. 3a, the graphene sheets clearly appear with small particles of TiO_2 nanoparticle distributed on its surface. Moreover, Fig. 3b shows denser surface coverage with a good distribution of TiO_2 and Ag nanoparticles.

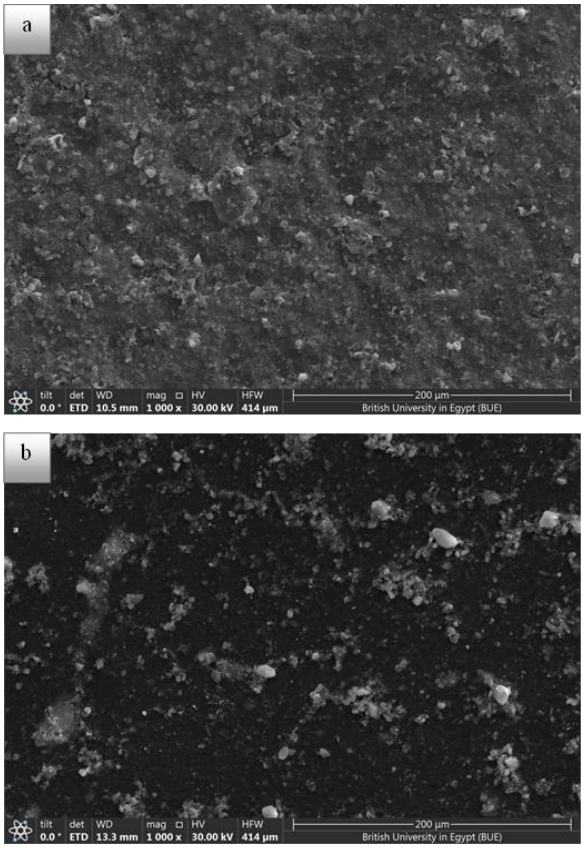

Figure 2. FE-SEM images of a) GC/G-TiO_2 electrode and b) GC/G-TiO_2-Ag electrode.

Figure 3c shows the elemental analysis for the modified electrodes. It can be observed the presence of fluorine peak which can be attributed to the presence of Nafion. The elemental analysis for both electrodes confirms the presence of G-TiO_2 and G-TiO_2-Ag on the electrode surface. In case of G-TiO_2, the elements percentage was C (22.49%), O (29.37%), F (26.11%) and Ti (22.02%). In case of G-TiO_2-Ag, the elements percentage was C (31.07%), O (24.35%), F (32.6%), Ag (3.2%), Ti (8.78%).

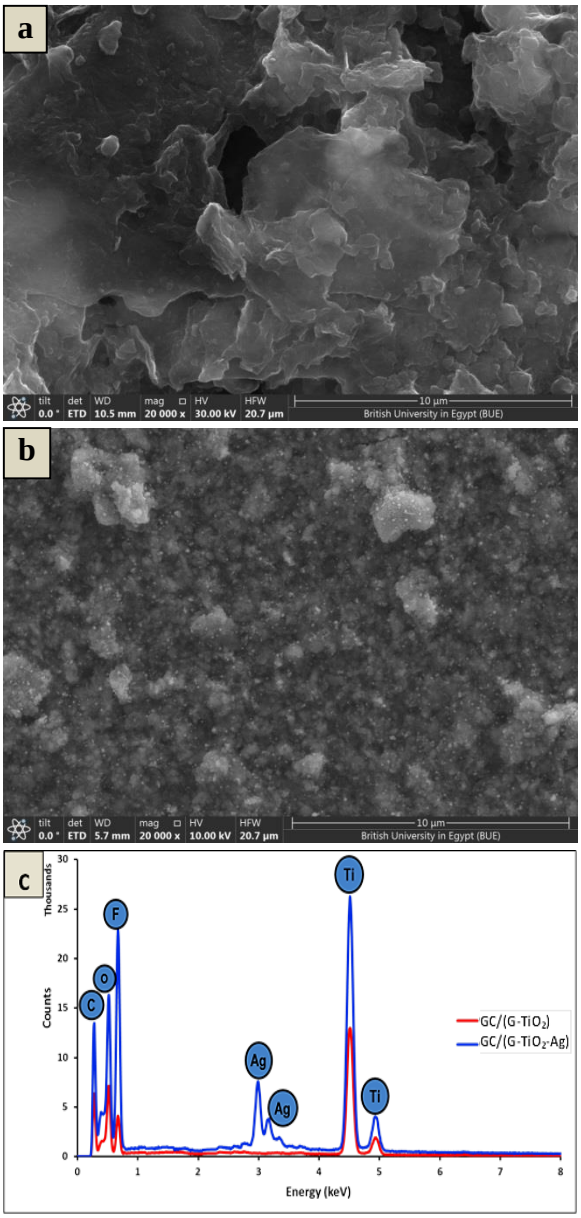

Figure 3. High magnification of FE-SEM image for the graphene sheets decorated with a) TiO_2 on the GC surface in GC/G-TiO_2 electrode and with b) TiO_2 and Ag on the GC surface in GC/G-TiO_2-Ag electrode. c) EDX analysis for the GC modified electrodes (G-TiO_2 and G-TiO_2-Ag).

3.2. Electrochemical behavior of GC/G-TiO_2 and GC/G-TiO_2-Ag nanocomposites

The electrochemical response of the bare GC electrode and GC modified with G-TiO_2 and G-TiO_2-Ag nanocomposites electrodes toward DO were demonstrated by cyclic voltammetry at scan rate of 50 mVs^{-1}. Phosphate buffer solution (PBS) of 0.1M concentration and pH 7.0 pH is used in the whole study.

Generally, ORR mechanism involves a series of electron transfer processes depends on the type of catalyst. Two different pathways, namely 2-electron (equations 1 and 2) and 4-electron (equation 3) pathways as follows:

$$O_2 + 2H^+ + 2e^- \rightarrow H_2O_2 \quad (1)$$

$$H_2O_2 + 2H^+ + 2e^- \rightarrow 2H_2O \quad (2)$$

$$O_2 + 4H^+ + 4e^- \rightarrow 2H_2O \quad (3)$$

The rate determining step of ORR is the adsorption of oxygen on the catalyst surface before its reduction hydrogen peroxide and H_2O [68], and this occurs on a metal catalyst like Ag [69]. In this work, composite catalysts prepared in nano-sizes and used to improve the kinetic of the electron transfer process between DO and the electrode surface.

Figures 4 represents the cyclic voltammetry of the bare GC electrode (A), GC/G-TiO_2 electrode (B), and GC/G-TiO_2-Ag (C) modified electrode, respectively in 0.1 M PBS (pH 7.0) N_2-saturated (a) and O_2-saturated (b), respectively. For CV in N_2-saturated solutions (Figs (4a), there are no obvious reduction peaks are detected, while different responses in O_2-saturated solutions are observed (Figs. 4(A-C) b. Two small peaks hardly detected at potentials of (-0.350V, -0.591V) and at -0.838 µA cm^{-2}, -1.214 µA cm^{-2} for DO reduction on GC electrode (Fig.4A (b). Also, two reduction peaks of relatively high current densities are observed for DO reduction on the surface of GC/G-TiO_2 electrode (Fig. 4B (b) at -0.569 and -0.386 V and at -29.25 µA cm^{-2}, and -21.57 µA cm^{-2}. These peaks can be attributed to the two steps four electron (4e`) mechanism for DO reduction [70]. According to the published mechanism [11], the first peak at – 0.386 V could due to the reduction of O_2 to H_2O_2 and OH^-, while, the second reduction peak at – 0.569 V is referred to the reduction of H_2O_2 to OH^-, The reduction peaks are slightly shifted to more positive potentials than that reported in literatures, this could attribute to the high surface area of the electrode which leads to increasing the number of active sites and improving the electrocatalytic activity [11].

Moreover, the oxygen of TiO_2, could help in oxidizing the intermediates formed during ORR thus help complete reduction of intermediates and reduce the catalyst poisoning as reported in the following reactions [25].

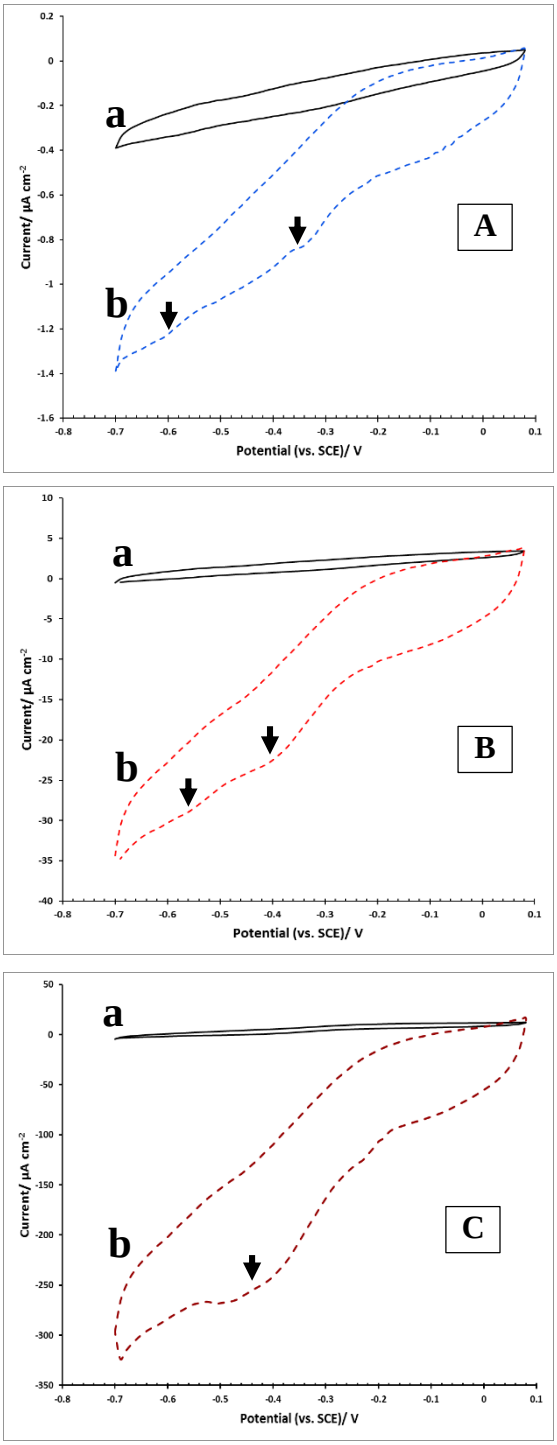

Figure 4. Cyclic voltammetry for the GC electrode (A), GC/G-TiO_2 (B) and GC/G-TiO_2-Ag (C) in PBS pH 7.0, a) N_2-saturated and b) O_2-saturated.

$$TiO_2 + H^+ + e^- \rightarrow TiO\text{-}OH \quad (4)$$

$$2TiO\text{-}OH + O_2 \rightarrow ((TiO\text{-}OH)O_{ads})_2 \quad (5)$$

$$((TiO\text{-}OH)O_{ads})_2 + e^- + H^+ \rightarrow (TiO\text{-}OH)O_{ads} + H_2O + TiO_2 \quad (6)$$

$$(TiO\text{-}OH)O_{ads} + e^- + H^+ \rightarrow TiO_2 + H_2O \quad (7)$$

However, the GC modified with G-TiO_2-Ag as shown in Fig. 4C, only one obvious peak at -0.429V with high peak current density (-267.45 µA cm^{-2}).

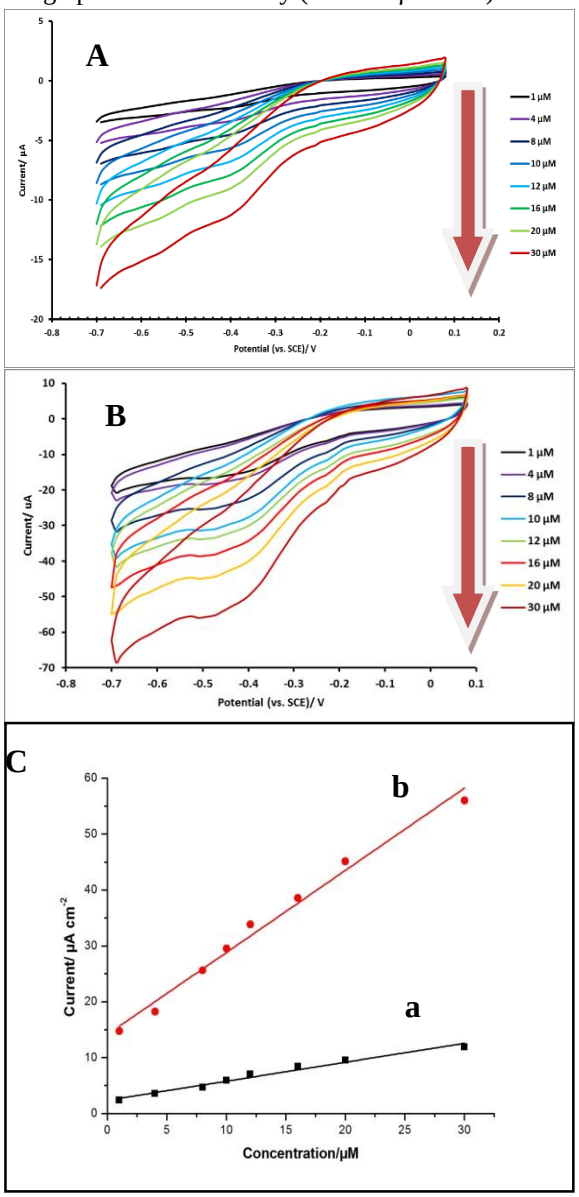

Figure 5. Cyclic voltammetry of (A) GC/G-TiO_2 and (B) GC/G-TiO_2-Ag modified electrode in PBS (pH 7) for different DO concentration (from 1 to 30 µM). (C) The relation between the reduction peak current of DO at various concentrations in PBS (pH 7) at 50 mV s^{-1} for: a) GC/G-TiO_2 and b) GC/G-TiO_2-Ag.

This strongly reflects that the reaction over the GC/ G-TiO_2-Ag is fast and efficient for one step (4e`) DO reduction. The difference in sensitivity between the two modified electrodes maybe attributed to the presence of Ag nanoparticles enhancing the catalytic effect of the electrode [71, 72]. Furthermore, the presence of Ag nanoparticles enhances the transformation of H_2O_2 to OH^- [71, 72].

It was reported that Ag is maintained in its metallic state during ORR, demonstrates excellent HO_2^- elimination oxidation, moreover Ag shows weak binding of ORR intermediates [27-30]. Thus, synergistic effects could occur in GC/G-TiO_2-Ag between Ag and TiO_2 lead to a higher catalytic activity towards ORR. As a result, a modification of the electronic structure of the components could occur and cooperation between the constituents of the catalyst for ORR is possible. The ORR may proceed via 2e pathway on one component and on another the peroxide formed can be further reduced [73]. The electrocatalytic activity of GC/G-TiO_2 and GC/G-TiO_2-Ag electrodes was examined for various DO concentrations as shown in Fig. 5 (A and B). It is clear that as the DO concentration increase from 1 to 30 µM, the electrocatalytic current of ORR increase.

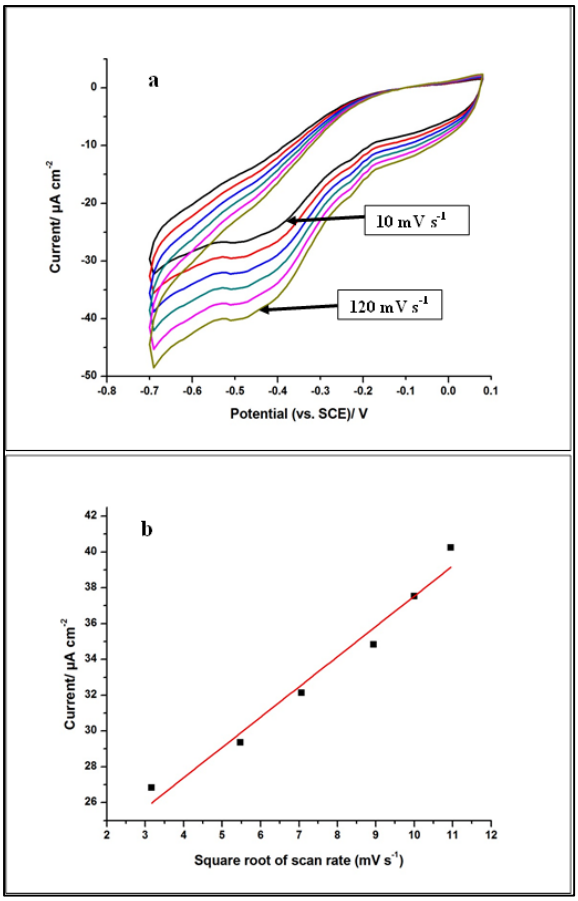

Figure 6. a) Cyclic voltammetry of GC/G-TiO_2-Ag modified electrode in PBS (pH 7) O_2 - saturated at different scan rate/ (10, 30, 50, 80, 100 and 120 mV s^{-1}) and b) The linear relation between the peaks currents with the square root of scan rate.

Figure 5C shows the relationship between the reduction peak current of DO and oxygen concentrations in 0.1 M PBS (pH 7.0) at GC/G-TiO_2 and GC/G-TiO_2-Ag electrodes at all concentrations range studied. It is worth noting that GC/G-TiO_2-Ag

electrode displayed a higher reduction peak current for DO at various concentrations compared with that of GC/G-TiO_2 electrode. The superior behavior displayed by GC/G-TiO_2-Ag electrode could due to the high surface area of GC/G-TiO_2-Ag electrode which increases the number of active sites and the catalytic activity.

Fig. 6 shows the electrocatalytic behavior of GC/G-TiO_2-Ag electrode at different scan rates from 10 to 120 mVs^{-1}. The DO reduction peak current increases gradually with the increase of the scan rate (Fig. 6a). Moreover, from Fig. 6b, the increase in the reduction peak current is proportional to the square root of scan rate, confirming that the reduction process is a diffusion controlled process, which is in a good agreement with the theoretical model reported by Andrieux and Saveant [74].

In order to estimate the no. of electron transferred (n) in the ORR the relation between the cathodic peak potential (E_{pc}) and ln V(scan rate) is plotted (Fig. 7) according to the following equation (8) [75]:

$$\mathbf{E_{pc} = E^{o} + RT/\alpha\, nF \times \ln(\alpha\, nF\upsilon/RTks)} \quad (8)$$

The relation indicates a straight line with slope equals (RT/ α nF) and the value of α n= 1.8208; where R is the universal gas constant (8.314 J $mol^{-1}K^{-1}$), T is the absolute temperature in Kelvin, F is Faraday's constant (96500 $Cmol^{-1}$), n is the electron transfer number, α charge transfer coefficient, its value (1> α > 0), whereas α = 0.5 in case of a reversible process and its value deviates from 0.5 in case of an irreversible process. Assuming that α= 0.5, the no. of electrons (n) will equal 3.6 ≈ 4 which is consistent with our proposed mechanism.

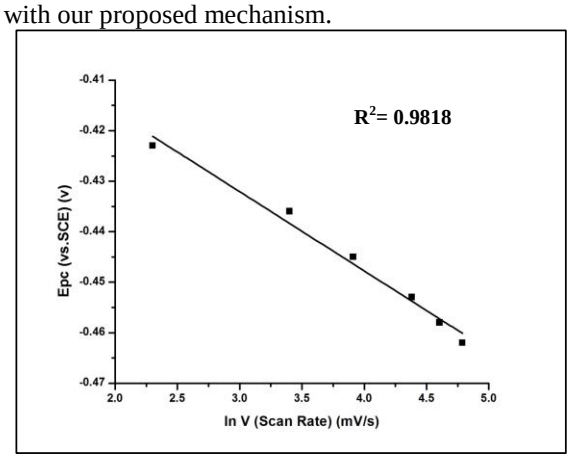

Figure 7. The relation between cathodic peak potential (E_{pc}) and ln V (scan rate).

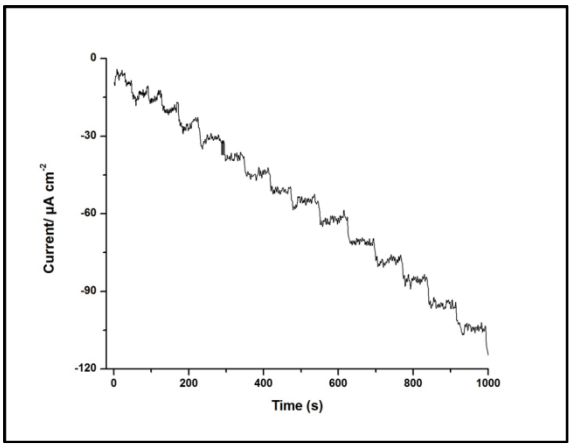

Figure 8. Amperometric response for the dissolved oxygen reduction on GC/G-TiO_2-Ag modified electrode in PBS (pH 7) for concentrations of; 1, 4, 8, 12, 16, 20, 25, 30, 40, 50, 60, 70, 80, 100 µM. Applied potential: -300 mV.

3.3. Amperometric study of GC/G-TiO_2-Ag electrode

In order to determine the sensitivity of GC/G-TiO_2-Ag electrode, the dissolved oxygen concentration had been determined first using the amperometric detection technique (Fig. 8). It is performed in PBS (pH 7) with continuous stirring and at applied voltage of -300 mV. The PBS solution was purged with highly pure nitrogen gas for 30 min before the measurement and different concentrations of dissolved oxygen were added sequentially. From Fig. 8, it is clear that a rapid and fast response is observed (reached to the steady state in around 5 s) for each successive addition of the DO. The calibration curve of the DO sensor was shown in Fig. 9. There are two linear response regions were noticed. In the first linear region, the current response increases rapidly with increase of DO concentration in the range from 1 µM to 30.29 µM (correlation coefficient 0.996) with sensitivity of 1.363 $\mu Acm^{-2}\ \mu M^{-1}$ and detection limit of 0.011 µM (signal/noise ratio = 3).

The second linear region shows an increase in response, with slow rate than the first region, for DO concentration up to 100 µM (correlation coefficient 0.990) with sensitivity of 0.725 $\mu Acm^{-2}\ \mu M^{-1}$ and detection limit of 0.214 µM (signal/noise ratio = 3). In both regions, the sensitivity was higher and better than those reported elsewhere as shown in table (1).

Table 1 : Comparison on the determination of dissolved oxygen using different modified electrodes

Electrodes	linearity	Sensitivity	Detection limit	References
silver nanodendrites electrode	1.0 to 66.71 µM	0.169 µA uM^{-1}	0.043 µM	[11]
G-Ag/GCE	1 to 120 µM	0.205 µA uM^{-1}	0.031 mM	[76]
Iron picket-fence porphyrin on multiwalled carbon nanotube gold modified electrode	0.52 to 180 µM	0.0594 µA uM^{-1}	0.38 µM	[18]
Manganese (II) phthalocyanine/ porous SiO_2/SnO_2 electrode	0.806 (±0.406) − 0.147 (±3.72×10^{-2}) mM	0.147 µA uM^{-1}	7.0×10^{-4} mM	[14]
The poly(methylene blue) modified GCE	3.5–180.625 µM	-	1.156 µM	[77]
cobalt tetrasulphonated phthalocyanine immobilized in a poly-l-lysine film	6.25–250 µM	0.343 µA uM^{-1}	3 µM	[78]
G-TiO_2-Ag	1 - 30.29 µM (1st linear region)	1.363 µAcm^{-2} $µM^{-1}$	0.011 µM	This work
	30.29 - 100 µM (2nd linear region)	0.725 µAcm^{-2} $µM^{-1}$	0.214 µM	This work

It is obvious that the proposed sensor exhibited a good sensing performance when compared to the other dissolved oxygen sensors reported before **Table (1)**. The reason for that can be attributed to the high electrocatalytic ability and efficient electron transfer over the electrode surface due to the synergetic effect as discussed above.

To indicate long term stability and the reproducibility of the two prepared electrodes towards the detection of dissolved oxygen, chronoamperometric experiments for GC/G-TiO_2 and GC/G-TiO_2-Ag electrodes in O_2-saturated 0.1 M PBS were conducted at -400 mV (SCE) and represented in Fig. 10. It is clear that GC/G-TiO_2-Ag electrode delivers a high steady-state reduction current about 2.7 times that of GC/G-TiO_2. This is due to the synergy between Ag nanoparticles and TiO_2. Also, the steady state reduction current of DO on GC/G-TiO_2-Ag electrode reached faster (after 200 seconds) than that on GC/G-TiO_2 electrode (after 800 seconds) could due to the promoting effect of the Ag nanoparticles.

Also, the synergy between the TiO_2 and Ag nano-particles also improves the stability and increases the tolerance to poisoning by intermediate species. It was found that for GC/G-TiO_2-Ag and GC/G-TiO_2 electrodes during the potentiostatic polarization at -400 mV (SCE), no decay in the ORR current density is observed for both electrodes as the reduction current increases till it reached to a steady state as shown in Fig. 10.

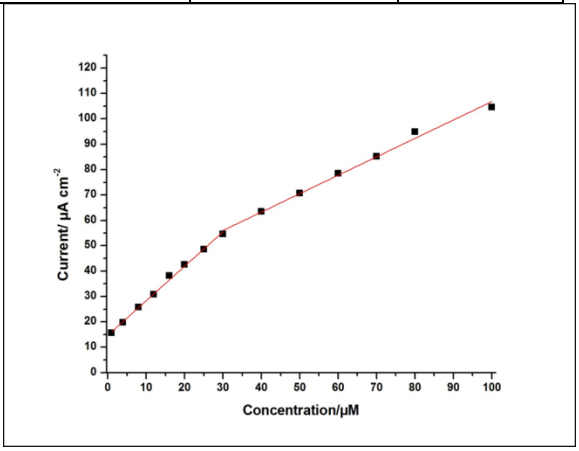

Figure 9. The calibration curve for GC/G-TiO_2-Ag modified electrode.

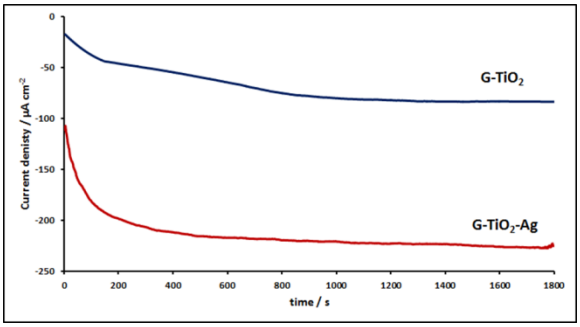

Figure 10. Chronoamperometry of G-TiO_2 and G-TiO_2-Ag electrodes at -400 mV (SCE) in O_2-saturated 0.1 M PBS.

The reproducibility of the prepared GC/G-TiO_2-Ag electrode was inspected for DO reduction at -400 mV (SCE) in O_2-saturated 0.1 M PBS at five prepared electrodes, and the relative standard deviation was found to 3.6 %. On the other side, the

prepared electrodes were stored in a dissector and tested for DO reduction every day. The retained catalytic activity was about 89 % of its original value after one week.

To investigate the specificity and selectivity of GC/GTiO$_2$-Ag electrode towards DO sensing, some common interfering species, such as ascorbic acid (AA), uric acid (UA), hydroquinone, SO_4^{2-}, NO_3^-, Na^+ and Ca^{2+} at 1.0 mM concentration each added at irregular intervals in 0.1 M PBS (pH 7.0) to measure the performance of selectivity under continuous stirring at the potential of −400 mV vs. SCE. No interference signals are observed at −400 mV vs. SCE and it was found weak response for such interfering species compared with DO response and the response ratios % were 3.8, 2.7, 4.1,3.2, 2.9, 1.9 and 2.5, for interfering species, respectively. The relatively weak response of GC/GTiO$_2$-Ag electrode sensor toward these interfering species (< 5 %) clarifies its specificity and selectivity towards ORR at this potential.

4. Conclusion

In the current work, G-TiO$_2$-Ag nanocomposite was successfully prepared hydrothermally. The modified glassy carbon electrode (GC) was obtained by the drop casting method. The proposed GC/G-TiO$_2$-Ag electrode exhibited good electrocatalytic activity toward the DO reduction, through one step four electron reaction, with high sensitivity, low detection limit and fast response. It also shows a small or even a null response toward some common interfering species at a potential of -400 mV (SCE). Accordingly, this ternary nanocomposite of graphene is recommended to be used in the development of the electrochemical DO sensor.

5. References

[1] Y. Wei, Y. Jiao, D. An, D. Li, W. Li, Q. Wei, Review of Dissolved Oxygen Detection Technology: From Laboratory Analysis to Online Intelligent Detection, Sensors 19(18) (2019).

[2] C.S. Martin, T.R.L. Dadamos, M.F.S. Teixeira, Development of an electrochemical sensor for determination of dissolved oxygen by nickel–salen polymeric film modified electrode, Sens. Actuators, B 175 (2012) 111-117.

[3] P. Zimmermann, A. Weltin, A.G. Urban, J. Kieninger, Active Potentiometry for Dissolved Oxygen Monitoring with Platinum Electrodes, Sensors 18(8) (2018).

[4] K.T. Tran-Ngoc, N.T. Dinh, T.H. Nguyen, A.J. Roem, J.W. Schrama, J.A.J. Verreth, Interaction between dissolved oxygen concentration and diet composition on growth, digestibility and intestinal health of Nile tilapia (Oreochromis niloticus), Aquaculture 462 (2016) 101-108.

[5] S. Wu, S. Wu, Z. Yi, F. Zeng, W. Wu, Y. Qiao, X. Zhao, X. Cheng, Y. Tian, Hydrogel-Based Fluorescent Dual pH and Oxygen Sensors Loaded in 96-Well Plates for High-Throughput Cell Metabolism Studies, Sensors 18(2) (2018).

[6] R.T. Bailey, F.R. Cruickshank, G. Deans, R.N. Gillanders, M.C. Tedford, Characterization of a fluorescent sol–gel encapsulated erythrosin B dissolved oxygen sensor, Anal. Chim. Acta 487(1) (2003) 101-108.

[7] T.M. Freeman, W.R. Seitz, AN OXYGEN PROBE BASED ON TETRAKIS ALKYL AMINOETHYLENE CHEMILUMINESCENCE11Partial Financial Support for this work was provided by NSF Grant CHE-7825192, in: M.A. Deluca, W.D. McElroy (Eds.), Bioluminescence and Chemiluminescence, Academic Press1981, pp. 347-349.

[8] Y. Suzuki, H. Nishide, E. Tsuchida, Membranes of the Picket Fence Cobalt Porphyrin Complexed with Poly(vinylimidazole and -pyridine)s: Selective Optical Response to Oxygen, Macromolecules 33(7) (2000) 2530-2534.

[9] B.J. Sanghavi, O.S. Wolfbeis, T. Hirsch, N.S. Swami, Nanomaterial-based electrochemical sensing of neurological drugs and neurotransmitters, Microchim. Acta 182(1) (2015) 1-41.

[10] D. Rao, X. Zhang, Q. Sheng, J. Zheng, Highly improved sensing of dopamine by using glassy carbon electrode modified with MnO_2, graphene oxide, carbon nanotubes and gold nanoparticles, Microchim. Acta 183(9) (2016) 2597-2604.

[11] D. Zhang, Y. Fang, Z. Miao, M. Ma, Q. Chen, Electrochemical determination of dissolved oxygen based on three dimensional electrosynthesis of silver nanodendrites electrode, J. Appl. Electrochem. 44(3) (2014) 419-425.

[12] X. Zhang, L.-X. Ma, Y.-C. Zhang, Electrodeposition of platinum nanosheets on C60 decorated glassy carbon electrode as a stable electrochemical biosensor for simultaneous detection of ascorbic acid,

dopamine and uric acid, Electrochim. Acta 177 (2015) 118-127.
[13] F.S. Damos, R.C.S. Luz, A.A. Tanaka, L.T. Kubota, Dissolved oxygen amperometric sensor based on layer-by-layer assembly using host–guest supramolecular interactions, Anal. Chim. Acta 664(2) (2010) 144-150.
[14] L.S.S. Santos, R. Landers, Y. Gushikem, Application of manganese (II) phthalocyanine synthesized in situ in the SiO_2/SnO_2 mixed oxide matrix for determination of dissolved oxygen by electrochemical techniques, Talanta 85(2) (2011) 1213-1216.
[15] L. Mao, K. Arihara, T. Sotomura, T. Ohsaka, A novel alkaline air electrode based on a combined use of cobalt hexadecafluoro-phthalocyanine and manganese oxide, Electrochim. Acta. 49(15) (2004) 2515-2521.
[16] Y. Lin, X. Cui, X. Ye, Electrocatalytic reactivity for oxygen reduction of palladium-modified carbon nanotubes synthesized in supercritical fluid, Electrochem. Commun. 7(3) (2005) 267-274.
[17] M. Zhang, Y. Yan, K. Gong, L. Mao, Z. Guo, Y. Chen, Electrostatic Layer-by-Layer Assembled Carbon Nanotube Multilayer Film and Its Electrocatalytic Activity for O_2 Reduction, Langmuir 20(20) (2004) 8781-8785.
[18] Y. Liu, Y.-L. Yan, J. Lei, F. Wu, H. Ju, Functional multiwalled carbon nanotube nanocomposite with iron picket-fence porphyrin and its electrocatalytic behavior, Electrochem. Commun. 9(10) (2007) 2564-2570.
[19] T. Getachew, F. Addis, S. Mehretie, H.-L. Yip, R. Xia, S. Admassie, Electrocatalytic reduction of oxygen at platinum nanoparticles dispersed on electrochemically reduced graphene oxide/PEDOT:PSS composites, RSC Adv. 10(51) (2020) 30519-30528.
[20] İ. Çakar, K.V. Özdokur, B. Demir, E. Yavuz, D.O. Demirkol, S. Koçak, S. Timur, F.N. Ertaş, Molybdenum oxide/platinum modified glassy carbon electrode: A novel electrocatalytic platform for the monitoring of electrochemical reduction of oxygen and its biosensing applications, Sens. Actuators, B 185 (2013) 331-336.
[21] Z.D. Wei, S.H. Chan, L.L. Li, H.F. Cai, Z.T. Xia, C.X. Sun, Electrodepositing Pt on a Nafion-bonded carbon electrode as a catalyzed electrode for oxygen reduction reaction, Electrochim. Acta. 50(11) (2005) 2279-2287.
[22] H. Ye, J.A. Crooks, R.M. Crooks, Effect of Particle Size on the Kinetics of the Electrocatalytic Oxygen Reduction Reaction Catalyzed by Pt Dendrimer-Encapsulated Nanoparticles, Langmuir 23(23) (2007) 11901-11906.
[23] M.S. El- Deab, T. Ohsaka, An extraordinary electrocatalytic reduction of oxygen on gold nanoparticles-electrodeposited gold electrodes, Electrochem. Commun. 4(4) (2002) 288-292.
[24] K. Ben Liew, W.R.W. Daud, M. Ghasemi, J.X. Leong, S. Su Lim, M. Ismail, Non-Pt catalyst as oxygen reduction reaction in microbial fuel cells: A review, International Journal of Hydrogen Energy 39(10) (2014) 4870-4883.
[25] X.-W. Liu, X.-F. Sun, Y.-X. Huang, G.-P. Sheng, K. Zhou, R.J. Zeng, F. Dong, S.-G. Wang, A.-W. Xu, Z.-H. Tong, H.-Q. Yu, Nano-structured manganese oxide as a cathodic catalyst for enhanced oxygen reduction in a microbial fuel cell fed with a synthetic wastewater, Water Research 44(18) (2010) 5298-5305.
[26] O. Lori, L. Elbaz Advances in Ceramic Supports for Polymer Electrolyte Fuel Cells, Catalysts 5(3) (2015).
[27] Y. Nie, L. Li, Z. Wei, Recent advancements in Pt and Pt-free catalysts for oxygen reduction reaction, Chemical Society Reviews 44(8) (2015) 2168-2201.
[28] A. Qaseem, F. Chen, X. Wu, R.L. Johnston, Pt-free silver nanoalloy electrocatalysts for oxygen reduction reaction in alkaline media, Catalysis Science & Technology 6(10) (2016) 3317-3340.
[29] R. Zhou, S.Z. Qiao, Silver/Nitrogen-Doped Graphene Interaction and Its Effect on Electrocatalytic Oxygen Reduction, Chemistry of Materials 26(20) (2014) 5868-5873.
[30] A. Holewinski, J.-C. Idrobo, S. Linic, High-performance Ag–Co alloy catalysts for electrochemical oxygen reduction, Nature Chemistry 6(9) (2014) 828-834.
[31] I. Kruusenberg, J. Leis, M. Arulepp, K. Tammeveski, Oxygen reduction on carbon nanomaterial-modified glassy carbon electrodes in alkaline solution, Journal of Solid State Electrochemistry 14(7) (2010) 1269-1277.
[32] K. Tammeveski, K. Kontturi, R.J. Nichols, R.J. Potter, D.J. Schiffrin, Surface redox catalysis for O2 reduction on quinone-modified glassy carbon electrodes, Journal of Electroanalytical Chemistry 515(1) (2001) 101-112.
[33] J.-J. Han, N. Li, T.-Y. Zhang, Ag/C nanoparticles as an cathode catalyst for a zinc-air battery with a flowing alkaline electrolyte, Journal of Power Sources 193(2) (2009) 885-889.
[34] R. Jiang, E. Moton, J.P. McClure, Z. Bowers, A Highly Active and Alcohol-Tolerant Cathode Electrocatalyst Containing Ag Nanoparticles

Supported on Graphene, Electrochimica Acta 127 (2014) 146-152.
[35] E.J. Lim, S.M. Choi, M.H. Seo, Y. Kim, S. Lee, W.B. Kim, Highly dispersed Ag nanoparticles on nanosheets of reduced graphene oxide for oxygen reduction reaction in alkaline media, Electrochemistry Communications 28 (2013) 100-103.
[36] J.M. Linge, H. Erikson, A. Sarapuu, M. Merisalu, M. Rähn, L. Matisen, V. Sammelselg, K. Tammeveski, Electroreduction of oxygen on nitrogen-doped graphene oxide supported silver nanoparticles, Journal of Electroanalytical Chemistry 794 (2017) 197-203.
[37] G. Aragay, F. Pino, A. Merkoçi, Nanomaterials for Sensing and Destroying Pesticides, Chemical Reviews 112(10) (2012) 5317-5338.
[38] S.U. Nanayakkara, J. van de Lagemaat, J.M. Luther, Scanning Probe Characterization of Heterostructured Colloidal Nanomaterials, Chemical Reviews 115(16) (2015) 8157-8181.
[39] A. Chen, C. Ostrom, Palladium-Based Nanomaterials: Synthesis and Electrochemical Applications, Chemical Reviews 115(21) (2015) 11999-12044.
[40] X. Zhu, Q. Jiao, X. Zuo, X. Xiao, Y. Liang, J. Nan, An Electrochemical Sensor Based on Carbon Nano-Fragments and β-cyclodextrin Composite-Modified Glassy Carbon Electrode for the Determination of Rutin, J. Electrochem. Soc. 160(10) (2013) H699-H703.
[41] G. Lu, L.E. Ocola, J. Chen, Reduced graphene oxide for room-temperature gas sensors, Nanotechnology 20(44) (2009) 445502.
[42] J.D. Fowler, M.J. Allen, V.C. Tung, Y. Yang, R.B. Kaner, B.H. Weiller, Practical Chemical Sensors from Chemically Derived Graphene, ACS Nano 3(2) (2009) 301-306.
[43] R. Kour, S. Arya, S.-J. Young, V. Gupta, P. Bandhoria, A. Khosla, Review—Recent Advances in Carbon Nanomaterials as Electrochemical Biosensors, Journal of The Electrochemical Society 167(3) (2020) 037555.
[44] S. Manavalan, U. Rajaji, S.-M. Chen, M. Govindasamy, S.S.P. Selvin, T.-W. Chen, M.A. Ali, F.M.A. Al-Hemaid, M.S. Elshikh, Sonochemical synthesis of bismuth(III) oxide decorated reduced graphene oxide nanocomposite for detection of hormone (epinephrine) in human and rat serum, Ultrason. Sonochem. 51 (2019) 103-110.
[45] C. Ben Ali Hassine, H. Kahri, H. Barhoumi, Enhancing Dopamine Detection Using Glassy Carbon Electrode Modified with Graphene Oxide, Nickel and Gold Nanoparticles, J. Electrochem. Soc. 167(2) (2020) 027516.
[46] M. Govindasamy, S.-M. Chen, V. Mani, M. Akilarasan, S. Kogularasu, B. Subramani, Nanocomposites composed of layered molybdenum disulfide and graphene for highly sensitive amperometric determination of methyl parathion, Microchim. Acta 184(3) (2017) 725-733.
[47] S. Pashazadeh, B. Habibi, Simultaneous Determination of Benzenediols Isomers Using Copper Nanoparticles/Poly (Glycine)/Graphene Oxide Nanosheets Modified Glassy Carbon Electrode, J. Electrochem. Soc. 167(16) (2020) 167504.
[48] X. Zhang, Y.-C. Zhang, L.-X. Ma, One-pot facile fabrication of graphene-zinc oxide composite and its enhanced sensitivity for simultaneous electrochemical detection of ascorbic acid, dopamine and uric acid, Sens. Actuators, B 227 (2016) 488-496.
[49] S. Manavalan, U. Rajaji, S.-M. Chen, T.-W. Chen, R.J. Ramalingam, T. Maiyalagan, A. Sathiyan, Q. Hao, W. Lei, Microwave-assisted synthesis of gadolinium(III) oxide decorated reduced graphene oxide nanocomposite for detection of hydrogen peroxide in biological and clinical samples, J. Electroanal. Chem. 837 (2019) 167-174.
[50] J. Hu, C. Zou, Y. Su, M. Li, X. Ye, B. Cai, E.S.-W. Kong, Z. Yang, Y. Zhang, Light-assisted recovery for a highly-sensitive NO_2 sensor based on RGO-CeO_2 hybrids, Sens. Actuators, B 270 (2018) 119-129.
[51] X. Yang, Y. Ouyang, F. Wu, Y. Hu, Y. Ji, Z. Wu, Size controllable preparation of gold nanoparticles loading on graphene sheets@cerium oxide nanocomposites modified gold electrode for nonenzymatic hydrogen peroxide detection, Sens. Actuators, B 238 (2017) 40-47.
[52] H. Ju, C. Shen, Electrocatalytic Reduction and Determination of Dissolved Oxygen at a Poly(nile blue) Modified Electrode, Electroanalysis 13(8-9) (2001) 789-793.
[53] M.W. Khalil, T.A. Salah Eldin, H.B. Hassan, K. El-Sayed, Z. Abdel Hamid, Electrodeposition of Ni–GNS–TiO_2 nanocomposite coatings as anticorrosion film for mild steel in neutral environment, Surf. Coat. Technol. 275 (2015) 98-111.
[54] D. Hariharan, P. Thangamuniyandi, A. Jegatha Christy, R. Vasantharaja, P. Selvakumar, S. Sagadevan, A. Pugazhendhi, L.C. Nehru, Enhanced photocatalysis and anticancer activity

of green hydrothermal synthesized Ag@TiO_2 nanoparticles, J. Photochem. Photobiol., B 202 (2020) 111636.

[55] M.S. Arif Sher Shah, K. Zhang, A.R. Park, K.S. Kim, N.-G. Park, J.H. Park, P.J. Yoo, Single-step solvothermal synthesis of mesoporous Ag–TiO_2–reduced graphene oxide ternary composites with enhanced photocatalytic activity, Nanoscale 5(11) (2013) 5093-5101.

[56] S.M. Silva, L.F. Aguiar, R.M.S. Carvalho, A.A. Tanaka, F.S. Damos, R.C.S. Luz, A glassy carbon electrode modified with an iron N4-macrocycle and reduced graphene oxide for voltammetric sensing of dissolved oxygen, Microchim. Acta 183(3) (2016) 1251-1259.

[57] H. Song, C. Ma, L. You, Z. Cheng, X. Zhang, B. Yin, Y. Ni, K. Zhang, Electrochemical hydrogen peroxide sensor based on a glassy carbon electrode modified with nanosheets of copper-doped copper(II) oxide, Microchim. Acta 182(7) (2015) 1543-1549.

[58] G. Ran, X. Chen, Y. Xia, Electrochemical detection of serotonin based on a poly(bromocresol green) film and Fe3O4 nanoparticles in a chitosan matrix, RSC Adv. 7(4) (2017) 1847-1851.

[59] Y.-J. Xu, Y. Zhuang, X. Fu, New Insight for Enhanced Photocatalytic Activity of TiO_2 by Doping Carbon Nanotubes: A Case Study on Degradation of Benzene and Methyl Orange, J. Phys. Chem. C 114(6) (2010) 2669-2676.

[60] F. Zou, Y. Yu, N. Cao, L. Wu, J. Zhi, A novel approach for synthesis of TiO_2–graphene nanocomposites and their photoelectrical properties, Scr. Mater. 64(7) (2011) 621-624.

[61] A.M. Shameli K, Zamanian A, Sangpour P, Parvaneh Shabanzadeh P, Abdollahi Y, Mohsen Z., Green Biosynthesis of Silver Nanoparticles using Curcuma Longa Tuber Powder., Int. J. Nanomedicine. 2012:7 (2012) 5603-5610.

[62] T. Ali, A. Ahmed, U. Alam, I. Uddin, P. Tripathi, M. Muneer, Enhanced photocatalytic and antibacterial activities of Ag-doped TiO_2 nanoparticles under visible light, Mater. Chem. Phys. 212 (2018) 325-335.

[63] P. Van Viet, N.C. Trung, P.M. Nhut, L. Van Hieu, C.M. Thi, The fabrication of the antibacterial paste based on TiO_2 nanotubes and Ag nanoparticles-loaded TiO2 nanotubes powders, J. Exp. Nanosci. 12(1) (2017) 220-231.

[64] L.C. Sim, K.H. Leong, S. Ibrahim, P. Saravanan, Graphene oxide and Ag engulfed TiO_2 nanotube arrays for enhanced electron mobility and visible-light-driven photocatalytic performance, J. Mater. Chem. A 2(15) (2014) 5315-5322.

[65] K. El-Sayed, Z.A. Hamid, T.A.S. Eldin, H.B. Hassan, Anti-Corrosion Nickel/Reduced Graphene Oxide-Titanium Dioxide Coating for Mild Steel in Organic Acids, J. Mater. Environ. Sci. 10(2, 2019) (2019) 141-162.

[66] K. Kotlhao, V.E. Pakade, F.M. Mtunzi, R.M. Moutloali, M.J. Klink, Preparation and Characterization of Ag–TiO_2 Modified Polyethersulfone (PES) Membranes for Potential Applications in Water Treatment, in: P. Ramasami, M. Gupta Bhowon, S. Jhaumeer Laulloo, H. Li Kam Wah (Eds.) Chemistry for a Clean and Healthy Planet, Springer International Publishing, Cham, 2019, pp. 331-349.

[67] S. AH, M. E, A. MB, G. V, Enhanced Bioactivity of Ag/ZnO Nanorods-A Comparative Antibacterial Study, J. Nanomed. Nanotechnol. 4(3, 168) (2013) 1-6.

[68] E. Yeager, Electrocatalysts for O2 reduction, Electrochimica Acta 29(11) (1984) 1527-1537.

[69] Z. Shi, J. Zhang, Z.-S. Liu, H. Wang, D.P. Wilkinson, Current status of ab initio quantum chemistry study for oxygen electroreduction on fuel cell catalysts, Electrochimica Acta 51(10) (2006) 1905-1916.

[70] W. Glasspool, J. Atkinson, A screen-printed amperometric dissolved oxygen sensor utilising an imobilised electrolyte gel and membrane, Sens. Actuators, B 48(1-3) (1998) 308-17.

[71] Y. Lu, Y. Wang, W. Chen, Silver nanorods for oxygen reduction: Strong effects of protecting ligand on the electrocatalytic activity, J. Power Sources 196(6) (2011) 3033-3038.

[72] A. Kongkanand, S. Kuwabata, Oxygen reduction at silver monolayer islands deposited on gold substrate, Electrochem. Commun. 5(2) (2003) 133-137.

[73] D.A. Slanac, A. Lie, J.A. Paulson, K.J. Stevenson, K.P. Johnston, Bifunctional Catalysts for Alkaline Oxygen Reduction Reaction via Promotion of Ligand and Ensemble Effects at Ag/MnOx Nanodomains, The Journal of Physical Chemistry C 116(20) (2012) 11032-11039.

[74] C. Andrieux, J. Savéant, Heterogeneous (chemically modified electrodes, polymer electrodes) vs. homogeneous catalysis of electrochemical reactions, 1978.

[75] E. Laviron, General expression of the linear potential sweep voltammogram in the case of diffusionless electrochemical systems, Journal of Electroanalytical Chemistry and Interfacial Electrochemistry 101(1) (1979) 19-28.

[76] L.I. Fu, Y. Zheng, Z. Fu, A. Wang, W.E.N. Cai, Dissolved Oxygen Detection by Galvanic

Displacement-Induced Graphene/Silver Nanocomposite, Bulletin of Materials Science 38(3) (2015) 611-616.

[77] X. Xiao, B. Zhou, L. Tan, H. Tang, Y. Zhang, Q. Xie, S. Yao, Poly(methylene blue) doped silica nanocomposites with crosslinked cage structure: Electropolymerization, characterization and catalytic activity for reduction of dissolved oxygen, Electrochim. Acta 56(27) (2011) 10055-10063.

[78] R.d.C.S. Luz, F.S. Damos, A.A. Tanaka, L.T. Kubota, Dissolved oxygen sensor based on cobalt tetrasulphonated phthalocyanine immobilized in poly-l-lysine film onto glassy carbon electrode, Sens. Actuators, B 114(2) (2006) 1019-1027.